Applied Catalysis B: Environmental 168-169 (2015) 87–97

Contents lists available at ScienceDirect

Applied Catalysis B: Environmental

journal homepage: www.elsevier.com/locate/apcatb

Ceria-supported Au–CuO and Au–Co_3O_4 catalysts for CO oxidation: An $^{18}O/^{16}O$ isotopic exchange study

N.K. Gamboa-Rosales[a], J.L. Ayastuy[a,*], Z. Boukha[a], N. Bion[b,**], D. Duprez[b], J.A. Pérez-Omil[c], E. del Río[c], M.A. Gutiérrez-Ortiz[a]

[a] Chemical Technologies for Environmental Sustainability Group, Department of Chemical Engineering, Faculty of Science and Technology, University of the Basque Country UPV/EHU, PO Box 644, E-48080 Bilbao, Spain
[b] Université de Poitiers, CNRS UMR7285, Institut de Chimie des Milieux et Matériaux de Poitiers (IC2MP), 4 rue Michel Brunet, TSA 51106, 86073 Poitiers Cedex 9, France
[c] Departamento de Ciencia de los Materiales, Ingeniería Metalúrgica y Química Inorgánica, Facultad de Ciencias, Universidad de Cádiz, Apartado 40, E-11510 Puerto Real (Cádiz), Spain

ARTICLE INFO

Article history:
Received 3 October 2014
Received in revised form
11 December 2014
Accepted 13 December 2014
Available online 16 December 2014

Keywords:
Isotopic exchange
Gold
Cobalt oxide
Copper oxide
Ceria
CO-PROX

ABSTRACT

In this work isotopic exchange of $^{18}O_2$ with ^{16}O and oxidation of $C^{16}O$ were investigated at 130 °C on ceria-supported Au–CuO and Au–Co_3O_4 catalysts. Oxygen storage capacity (OSC) was measured at 400 °C to check the influence of the metals in the catalysts, resulting in an enhancement of OSC for gold-containing catalysts compared to monometallic catalysts. The reactivity of surface oxygen atoms and the oxygen availability from the samples were studied by two isothermal experiments, both feeding $C^{16}O$ (anaerobic oxidation $C^{16}O$/Ar and aerobic oxidation $C^{16}O/O_2$) to the ^{18}O pre-exchanged samples. Exchange leads to $C^{18}O$ formation and oxidation leads to $C^{16}O_2$, $C^{16}O^{18}O$ and $C^{18}O_2$ formation. In anaerobic conditions the predominant reaction at the beginning is the exchange: a rapid exchange of $C^{16}O$ with the surface can be observed for all the samples except for CoCe that inhibits the exchange and the CO oxidation. In aerobic conditions, the predominant reaction is CO oxidation with the rapid increase of $C^{16}O_2$ due to the relatively high ^{16}O coverage in reaction as a result of the $C^{16}O$ exchange and from exchange between ^{18}O surface species and ^{16}O bulk atoms. At 130 °C, bare ceria shows null activity in both aerobic and anaerobic oxidation.

1. Introduction

Surface mobility phenomena of active species play an important role in catalysis, in the catalytic process itself as well as during activation or regeneration treatments of the catalysts. Steam reforming of hydrocarbons [1], the oxygen storage and release of three-way catalysts [2,3], remote control effect during selective oxidation [4] and reactions involving spillover of active species are well known examples where the migration of surface species can play a determining role in catalysis. The use of isotopic exchange studies is helpful for the elucidation of active surface species involved in the enhancement of catalytic activity.

$^{16}O/^{18}O$ exchange has been proven as a very useful technique to elucidate reaction mechanisms involving mobility of oxygen-containing reactive species [5,6], to study of the transient kinetics of surface and bulk oxygen diffusion in TWC [7], or to quantify the oxygen from the lattice wich participate in the WGS reaction via the "redox" route [8]. In essence, the method is based on the measurement of the rate of exchange between ^{18}O and ^{16}O species which could occur between gas phase and the support via metal particles, with small metallic clusters acting as portholes of oxygen on the support.

In this work we have focused our attention on ceria-supported gold catalysts modified with transition metal oxide (copper or cobalt) which have been reported as active for both CO-PROX and CO oxidation [9–11], with the aim of measuring the rate of exchange of $^{18}O/^{16}O$ species and to study the effect of the transition metal during the oxidation of carbon monoxide in the absence and in the presence of gas phase oxygen. On the other hand, for the gold-free CuO/CeO_2 and Co_3O_4/CeO_2 catalysts, the effect of the corresponding transition metal on the mobility of oxygen species on the catalyst surfaces has also been studied.

* Corresponding author. Tel.: +34 94 601 2619; fax: +34 94 601 5963.
** Corresponding author. Tel.: +33 5 49 45 36 44; fax: +33 5 49 45 37 41.
E-mail addresses: joseluis.ayastuy@ehu.es (J.L. Ayastuy), nicolas.bion@univ-poitiers.fr (N. Bion).

http://dx.doi.org/10.1016/j.apcatb.2014.12.020
0926-3373/

2. Experimental

2.1. Catalysts preparation

High surface area ceria (Rhodia, S_{BET} = 227 m^2/g) has been used as a support for all the samples (denoted latter as Ce). CuO/ceria catalyst (CuCe) was prepared by incipient wetness impregnation from aqueous solution of $Cu(NO_3)_2{\cdot}3H_2O$, then dried at 110 °C overnight and calcined in air at 500 °C for 5 h. Co_3O_4/ceria catalyst (CoCe) was prepared by the deposition precipitation method from aqueous solution of $Co(NO_3)_2{\cdot}6H_2O$, at pH 8 and 80 °C, then dried at 110 °C overnight and calcined in air at 500 °C for 5 h. Also, the Au/ceria catalyst (AuCe) was prepared by deposition precipitation from an aqueous solution of $HAuCl_4.3H_2O$, at pH 8 and 80 °C; after aging during 2 h, the solid was filtered and washed with distilled water at 90 °C, dried overnight at 110 °C in air, and finally calcined at 350 °C for 3 h. For the pH adjusting a solution of Na_2CO_3 was used (0.5 M).

In Au–CuO/CeO_2 and Au–Co_3O_4/CeO_2 catalysts (denoted as AuCuCe and AuCoCe, respectively), gold was deposited on previously prepared monometallic samples by the deposition precipitation method. The samples were dried overnight at 110 °C in air and calcined at 350 °C for 3 h. For all the gold-containing samples the nominal gold loading was 1 wt.%. The nominal content of copper and cobalt was 7 and 10 wt.%, respectively.

2.2. Characterization of catalysts

Specific surface area and pore size distribution of the samples were determined by N_2 adsorption–desorption isotherms at 78 K (MicromeriticsTristar 3000). Actual metal content was evaluated by atomic absorption spectroscopy (PerkinElmer A Analyst 800). The phase identification was carried out by XRD (Philips PW1710 diffractometer) using a finely ground powder sample applying CuKα radiation in continuous scan mode (2θ = 10–50°). PANalyticalX'pert High Score specific software was used for data interpretation, and the phases present in the samples were identified by comparing with the JCPDS Power Diffraction File (PDF) database. Crystallite sizes for the detected phases were estimated by means of the Scherrer equation. In addition, Williamson-Hall analysis of the diffraction peaks of ceria was done for all the samples. We do not taken into account the anisotropic effects.

Catalysts have also been characterized by means of High Resolution Transmission (HRTEM) and High-Angle Annular Dark Field–Scanning Transmission (HAADF–STEM) electron microscopies. HRTEM and STEM–HAADF images were obtained on a JEOL2010F instrument using a 0.5 nm electron probe at a camera length of 10 cm. The STEM–HAADF imaging mode provides contrasts directly related to the square average atomic number (Z) in the region under the electron beam. The difference in atomic number between Au (Z = 79) and support cations (Z_{Ce} = 58, Z_{Cu} = 29 and Z_{Co} = 27) is large enough as to guarantee optimum imaging of gold nanoparticles (Au–NP) with diameters even smaller than 1 nm for a small support thickness. From the contrasts observed in HAADF images, a discrimination of Au–NP and support can be performed. In any case, the nature of the particles included in the size distribution was further confirmed by X-ray energy dispersive spectroscopy (X-EDS) in STEM mode. The JEOL 2010F microscope used has a structural resolution of 0.19 nm at Scherzer Defocus conditions at 200 kV and it was equipped with a HAADF detector, an EELS spectrometer (GIF2000 Gatan Imaging Filter), and a X-EDS, Oxford Xmax (80mm2) SDD detector. Electron microscopy data were processed using Digital Micrograph. Eje-Z software, developed at the University of Cádiz, were used for the interpretation of HRTEM images [12]. To avoid any contact with solvents, samples for electron microscopy studies were prepared by depositing small amounts of the catalyst powder directly onto holey-carbon coated Mo grids. Excess powder was removed from the grids by gentle blowing with a nozzle.

The H_2-TPR experiments were carried out over pre-oxidized samples from −20 to 500 °C in a 5% H_2/Ar flow, with a heating ramp of 10 °C/min, and hydrogen consumption being continuously monitored by TCD. The oxygen storage capacity (OSC) of the samples was measured by a CO/O_2 pulse-injection method in an atmospheric glass fixed bed reactor placed in an electrical oven connected to a Porapak column and a TCD already described elsewhere [13]. The sample (c.a. 6 mg) was placed into the reactor and heated up to 400 °C under a helium flow at atmospheric pressure. At this temperature, 10 pulses (loop volume = 0.267 cm^3 STP) of pure O_2 were introduced, followed by sample purging into He flow for 10 min. Then, pulses of pure CO were injected until the area of CO peak was constant, before a new purging step of 10 min with He. The OSC probes the amount of oxygen immediately available in the materials while the oxygen storage complete capacity (OSCC) characterizes the total amount of reactive oxygen available in the oxide. On ceria-based samples a fraction of the amount of CO consumed results from the formation of carbonate species. The OSC and OSCC values are thus based on the amount of CO_2 produced which really represent the reduction of the catalyst with the first pulse of CO (OSC) or the first 10 pulses of CO (OSCC). On Au-containing catalysts CO may disproportionate to form CO_2 and C depending on the temperature of the measurement. The corresponding amount of CO_2 produced by this parallel reaction is subtracted from the total amount of CO_2 measured to determine the real OSC and OSCC values.

Catalysts were tested in CO-PROX reaction at 130 °C and O_2/CO lean conditions (λ = 0.48, defined as $2{\cdot}P_{O2}/P_{CO}$, which accounts the oxygen excess with respect to the stoichiometric for the complete CO oxidation, in the absence of parallel reactions) in a tubular reactor at WSV = 2.53 NL/min·g, with the following feed composition: CO/H_2/O_2 = 3.9/51.9/0.93 (He to balance). The outlet gas mixtures from the reactor were analyzed with a gas chromatograph system equipped with TCD detectors (MicroGC Agilent).

2.3. Isotopic exchange experiments

Isotopic exchange experiments were carried out in a closed recycle reactor, which is described elsewhere [14]. The connection of the system to the mass spectrometer was thermo-regulated to preserve a constant pressure of 10^{-6} mbar in the ionization chamber, while the total pressure in the reactor was around 53 mbar during the temperature programmed isotopic exchange (TPIE) experiments. Prior to TPIE, c.a. 20 mg of catalyst was placed into the reactor between two quartz wool plugs, pre-treated under an oxygen flow ($^{16}O_2$, 30 cm^3/min) for 1 h at 500 °C, cooled down to 200 °C under the same oxygen flow and finally subjected to outgassing for 30 min. A pure $^{18}O_2$ (99% of ^{18}O, Isotec) dose (53 mbar) was then introduced in the reactor, and the temperature increased from 200 °C to 600 °C at 2 °C/min. The partial pressure evolution for $^{16}O_2$ (m/z = 32), $^{16}O^{18}O$ (m/z = 34), $^{18}O_2$ (m/z = 36), $C^{18}O$ (m/z = 30), $C^{16}O_2$ (m/z = 44), $C^{16}O^{18}O$ (m/z = 46), and $C^{18}O_2$ (m/z = 48) were monitored every 4 s, and N_2 (m/z = 28) was also recorded to detect possible leaks. The total pressure ($P_{36} + P_{34} + P_{32}$) remained virtually constant.

$C^{16}O$ oxidation was investigated on the ^{18}O-exchanged samples in order to understand the reactivity of surface oxygen atoms. Experiments were carried out at 130 °C for all the samples. CO (6.6 mbar) was balanced with $^{16}O_2$ or Ar in order to obtain 53 mbar of total pressure.

From the variation in partial pressures, information on the rate of exchange (Re), the number of oxygen exchange (Ne) and the

type of exchange mechanism may be obtained [5]. These values are calculated from the following equations:

$$Re = -Ng \times \frac{d\alpha_g^t}{dt} \quad (1)$$

$$Ne = Ng \times (\alpha_g^0 - \alpha_g^t) \quad (2)$$

where Ng is the total number of oxygen atoms in the gas phase, α_g^t is the atomic fraction of ^{18}O in the gas phase at time t, and α_g^0 is the initial atomic fraction of ^{18}O in the gas phase.

The mechanisms for the oxygen exchange are described by the following equations [15]:

Simple heteroexchange:

$$^{18}O^{18}O_{(g)} + ^{16}O_{(s)} \rightarrow {}^{18}O^{16}O_{(g)} + ^{18}O_{(s)} \quad (3)$$

Multiple heteroexchange:

$$^{18}O^{18}O_{(g)} + 2^{16}O_{(s)} \rightarrow {}^{16}O_{2(g)} + 2^{18}O_{(s)} \quad (4)$$

where subscripts (s) and (g) correspond to the catalyst surface and gas phase, respectively. Both mechanisms involve the following three steps: (i) dissociative adsorption of molecular oxygen; (ii) exchange of the adsorbed atoms with atoms from the oxide; and (iii), associative desorption of molecular oxygen from the oxide surface. The occurrence of simple or multiple heteroexchange mechanisms could be differentiated at the beginning of the reaction (i.e., far from the gas/solid equilibrium) in isothermal or TPIE conditions by checking the initial appearance of $^{18}O^{16}O$ or $^{16}O_2$ in the gas phase, respectively. In order to evaluate the error range in a measurement using the isotopic exchange technique, an experiment has been repeated 5 times maintaining exactly the same conditions in terms of temperature, mass of catalyst, and initial $^{18}O_2$ pressure. The percentage of error has been calculated on the number of exchanged atoms and on the initial rate of exchange. Hence it took into account the errors due to the weighing, the temperature measurement, the $^{18}O_2$ pressure measurement, the intensities of the 36, 34 and 32 m/z collected. We obtained the following percentages: 2.98% for the number of atoms exchanged (Ne and $Ne_{,total}$), and 6.46% for the rate of exchange (Re).

3. Results and discussion

3.1. Catalyst characterization

Some of the textural properties of the samples are listed in Table 1. BET surface area slightly decreases when gold is deposited onto ceria. On the other hand, the copper or cobalt addition resulted in a significant decrease of the specific surface area, probably as a consequence of the sintering of ceria assisted by the transition metal oxide [16]. However, there is little difference in BET specific surface area among copper- and cobalt-based samples. There may be sintering of the ceria-supported gold catalysts and segregation in supported-phases, especially in the cobalt oxide–ceria sample. These two mechanisms are, however, not mutually exclusive and might occur simultaneously. The observed crystallite size for ceria was around 7 nm, calculated by XRD using the Scherrer equation, which does not significantly change after addition of any metal. In addition, the Williamson-Hall analysis for ceria says that, independent of the kind of metal deposited onto ceria (Au, Co or Cu, individually or combination of them), the crystallite sizes of ceria remains almost constant (around 5–7 nm). The same results were found by electronic microscopy analysis, as discussed below. None of copper-containing samples show diffraction peaks corresponding to CuO or Cu_2O, suggesting that copper species are highly dispersed on the support or they are in an amorphous state. The diffraction peaks of cobalt can be indexed to the spinel form of the Co_3O_4 (JCPDS 42-1467) in cobalt-containing samples, with a mean crystallite size of 13.2 nm for CoCe sample, which slightly decreases after gold deposition to 11.1 nm. For gold-containing samples the absence of diffraction peaks for gold species indicated that Au is finely dispersed on the samples, with primary particle sizes between 2 and 7 nm, as measured by HAADF–STEM (Table 1).

To gain some further insight into the nanostructural characterization of the catalysts, Figs. 1 and 2 summarize some relevant observations deduced from the analysis of the HAADF–STEM and HRTEM images. According to Fig. 1A, HAADF–STEM images and the composition nanoanalysis of Co-containing catalyst suggest that cobalt oxide was highly segregated from the ceria support. HRTEM images show heterogeneous Co_3O_4 particles in the 20–115 nm size range with an average particle diameter of about 50 nm. Small Au–NPs supported on ceria were detected in HAADF–STEM images, in particular from 2 to 3 nm in diameter. In some cases, the nature of the NP has to been confirmed by X-EDS analysis. In most cases, these gold nanoparticles were supported on ceria, which in turn, was found on many occasions as conglomerates on Co_3O_4. In this respect, in lower frequency gold nanoparticles of about 6–7 nm were supported on Co_3O_4. The HAADF–STEM micrographs, in the case of the AuCuCe catalyst (Fig. 1B), suggest that the copper oxide phase was highly dispersed on ceria (with an average size of 5.1 nm), which was confirmed by X-EDS nanoanalysis. CuO particles of relatively large size were not found, suggesting high homogeneity in the supported copper oxide particles on CeO_2 support. Nevertheless, the observed gold nanoparticles supported on ceria were larger than in the case AuCoCe sample, of about 5–7 nm.

HRTEM analysis (Fig. 2) confirmed cobalt oxide particles segregated from ceria, with very high heterogeneity. As shown in Fig. 2A, HRTEM results also indicate the poor-dispersion of cobalt oxide. In contrast, the primary particle size of CeO_2 ranged between 5 and 10 nm, in good agreement with XRD. In addition, the structural features of these crystals as determined by digital diffraction analysis of experimental micrographs (HRTEM). Fig. 2B shows the

Table 1
Textural properties, chemical composition, and redox properties. Total and real OSC and OSCC in $\mu mol_O/g_{cat}$.

Bulk composition (at./at.)							d_{Au}(nm)	OSC		OSCC	
Catalyst	S_{BET} (m^2/g_{cat})	Au (wt.%)	Au/Ce ($\times 10^3$)	Cu/Ce	Co/Ce	Au/(Me)[a] ($\times 10^3$)		Total	Real[d]	Total	Real[d]
Ce	226	0	–	–	–	–	–	219	219	300	300
AuCe	219	0.8	7.1	–	–	7.1	6.0	410	350	463	402
CuCe	125	0	–	0.23	–	–	–	1737	196	2037	496
AuCuCe	105	1.0	9.7	0.25	–	7.8	5–7	2280	578	2502	800
CoCe	112	0		–	0.36	–	–	1022	264	1587	829
AuCoCe	103	0.7	6.7	–	0.24	5.4	2–3 [b] 6–7 [c]	1329	760	1780	1213

[a] Me = Cu + Co + Ce.
[b] Au particles supported on ceria.
[c] Au particles supported on cobalt oxide (From HAADF-STEM).
[d] Real OSC and OSCC are obtained considering the metal completely oxidized (CuO, Co_3O_4 and Au_2O_3) before the first CO pulse and removing from total OSC and OSCC the contribution due to the reduction of the metal oxide.

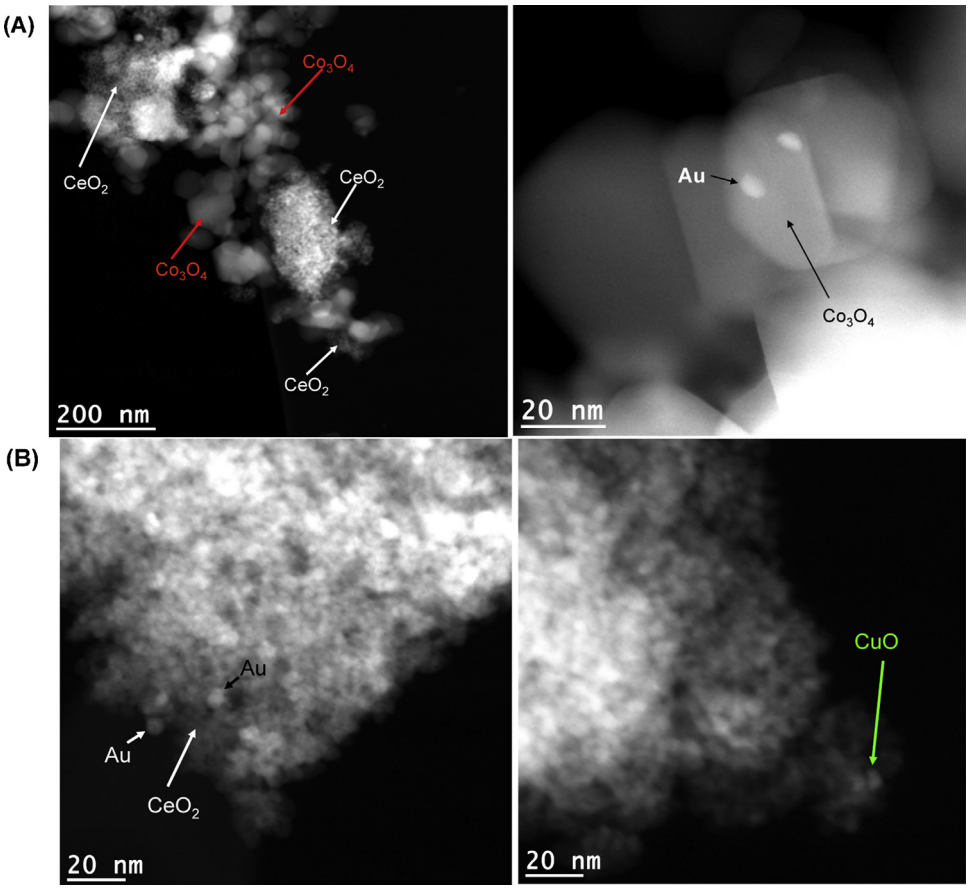

Fig. 1. HAADF-STEM images of (A) AuCoCe and (B) AuCuCe catalysts.

digital diffraction pattern (DDP) corresponding to a ceria crystal. Likewise, the inset in this figure shows spots which correspond to sets of atomic planes of the crystalline structure. These results revealed that CeO_2 particle may be distinctly interpreted as cubic fluorite geometry along the [0 1 1] zone axis. Also, in good agreement with XRD data, HRTEM results confirmed the stoichiometric spinel structure for Co_3O_4 phase, Fig. 2C. As shown in this Figure, the geometrical arrangement of the different reflections (inset) corresponds to the [0 1 1] zone axis of this phase. The values of 4.09 Å and 4.69 Å may be respectively assigned to the *d*-spacing of (2 0 0) and (1 1 −1) family planes of spinel-Co_3O_4 phase.

Fig. 3A shows the H_2-TPR profiles obtained for all the samples, while Fig. 3B shows the cumulative hydrogen uptake, were have been allocated the various phases present in the materials in function of temperature, assuming that at the beginning gold, copper and cobalt are essentially as Au_2O_3 [17,18], CuO and Co_3O_4, respectively. For pure ceria, two reduction peaks are detected in H_2-TPR, the low temperature peak (at 490 °C) and high temperature peak (at about 834 °C) corresponding to the reduction of surface of ceria and bulk ceria, respectively. The AuCe sample shows a single reduction peak at 132 °C, which amounts 840 $\mu mol_{H2}/g_{cat}$, larger than the theoretical consumption for the complete reduction of

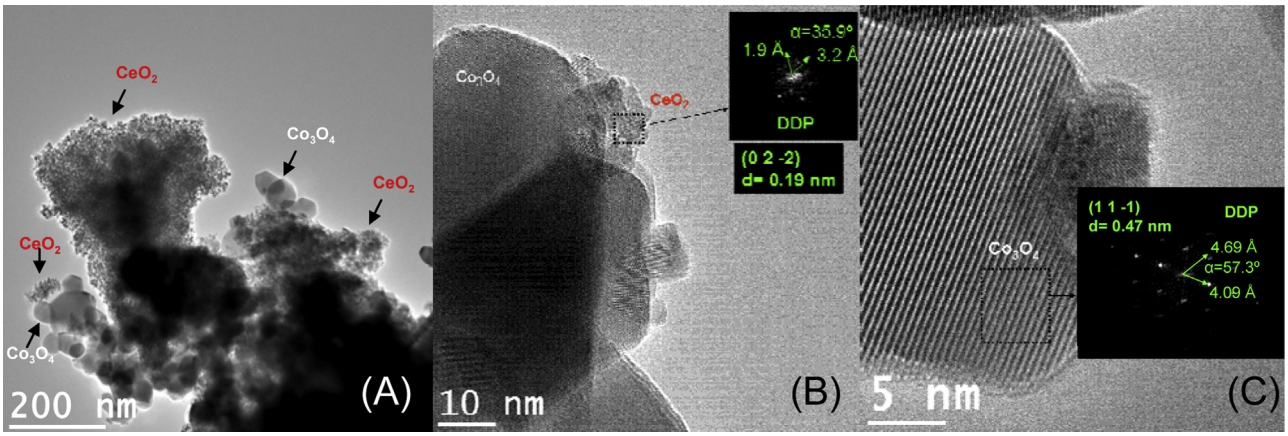

Fig. 2. TEM images of the AuCoCe sample. (A) A low-magnification microimage of the catalyst. HRTEM images of (B) a small ceria particle (~5 nm in diameter) and (C) a bigger crystal of Co_3O_4 (~25 nm in diameter). The insets in the images correspond to the digital diffraction patterns (DDP's) of a selected area, where the measured d spacing account for the family planes, (0 2 −2) and (1 1 −1) of the CeO_2 and Co_3O_4 phases, respectively.

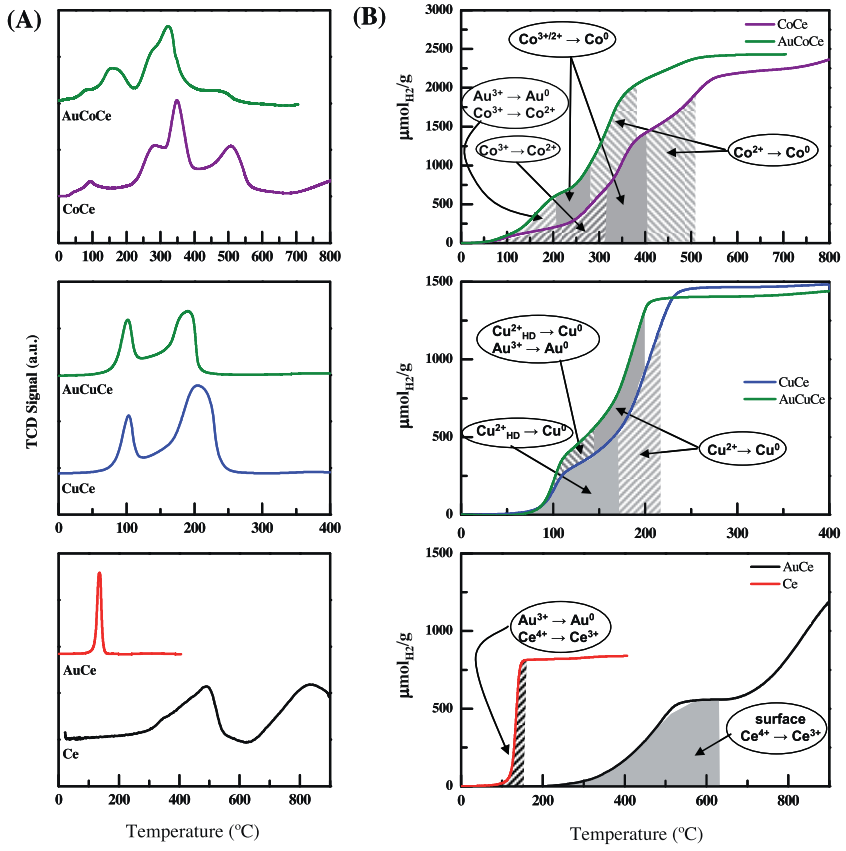

Fig. 3. (A) Temperature-programmed reduction profiles of Ce, AuCe, CuCe, AuCuCe, CoCe and AuCoCe samples; (B) Cumulative hydrogen uptake and phase allocation.

Au^{3+} species, suggesting that this reduction peak corresponds to the simultaneous reduction of oxygen species of cationic gold and the surface of ceria [19]. The CuCe sample shows two well-defined peaks: the low temperature peak, centered at 100 °C, is related to the reduction of small, highly dispersed copper species in intimate contact with ceria (symbolized as $Cu^{2+}{}_{HD}$ in the Fig. 3B) [20], while the reduction peak at higher temperature corresponds to the simultaneous reduction of less dispersed copper species, bulk CuO and the surface layers of ceria [21], as the total hydrogen consumption (1484 $\mu mol_{H2}/g_{cat}$) exceeds the corresponding consumption for the reduction of CuO.

The reduction profile of the AuCuCe sample shows at least two reduction peaks: the low temperature peak at 101 °C (which amounts to 521 $\mu mol_{H2}/g_{cat}$), and a broader one at 190 °C (which amounts to 920 $\mu mol_{H2}/g_{cat}$). In addition, the absence of a clear, separated peak for reduction of cationic species of gold suggests the simultaneous reduction of both highly dispersed copper species ($Cu^{2+}{}_{HD}$) and oxygen species of gold (in the low temperature peak), and bulk CuO and surface ceria (in the high temperature peak). Compared to the AuCe sample, the lowering of the reduction temperature for gold species indicates some promotion in the reduction of gold species by highly dispersed copper species.

The peak assignment for the reduction of CoCe sample was the following [22]: the peak at 102 °C corresponds to the reduction of the surface adsorbed oxygen species; the peak at 292 °C is ascribed to the reduction of Co^{3+} to Co^{2+} at the interface between Co_3O_4 and ceria; the peak at 353 °C corresponds to the reduction of Co_3O_4 weakly interacting with ceria to metallic Co; the peak at 517 °C can be attributed to the reduction of Co^{2+} interacting with ceria to metallic Co; and finally, at $T > 700$ °C, the reduction of the bulk of ceria. As the measured hydrogen uptake (2624 $\mu mol_{H2}/g_{cat}$) exceeds the corresponding theoretical for $Co_3O_4 \rightarrow Co^0$ reduction, the simultaneous reduction of surface ceria layers and cobalt species should be concluded.

After addition of Au, the reduction peaks of cobalt species shift to lower temperature for the AuCoCe sample. The peak at 88 °C corresponds to the reduction of the surface adsorbed oxygen species. The reduction from Co^{3+} to Co^{2+} at the ceria–cobalt oxide interface occurs at 150 °C, and the subsequent reduction from Co^{2+} to metallic Co at 330 °C. The shoulder at 481 °C corresponds to the reduction of the surface of ceria.

Both total and real OSC and OSCC of all the samples, measured at 400 °C, are also reported in Table 1. The real OSC and OSCC values due to the ceria support were obtained assuming that the corresponding metals were completely oxidized after oxidizing pre-treatment (that is, they are as CuO, Co_3O_4 and Au_2O_3 on the ceria surface [17] and completely reduced after the first CO pulse (assuming the following reduction reactions: $CuO \rightarrow Cu^0$; $Au_2O_3 \rightarrow Au^0$; $Co_3O_4 \rightarrow Co^0$). Accordingly, we subtracted from the total OSC and OSCC values the contribution due to the reduction of the metal oxides, which amounts to 60 $\mu mol_O/g$ for AuCe; 1541 $\mu mol_O/g$ for CuCe; 1702 $\mu mol_O/g$ for AuCuCe; 758 $\mu mol_O/g$ for CoCe; and 569 $\mu mol_O/g$ for AuCoCe.

It is observed that the total OSC increases with the incorporation of gold. For example, the total OSC of bare ceria increases of 191 $\mu mol_O/g$ after gold incorporation (AuCe catalyst). For gold-containing catalysts, the total OSC increment caused by gold is even larger than the observed for monometallic catalyst (increase of 543 $\mu mol_O/g$ for AuCuCe with respect to the CuCe and in 307 $\mu mol_O/g$ for AuCoCe with respect to CoCe), which suggests a synergistic effect in the interface between gold species and CuO or Co_3O_4 particles, stronger than in gold–ceria interface, specifically for AuCuCe sample, as shown by H_2-TPR. Strong interaction of gold with cobalt oxide has been already reported in literature [23]. Also,

it is suggested that gold weakens the Cu—O bond due to the strong interaction among gold and copper [24].

Similarly to the total OSC, the real OSC for gold-containing catalysts are higher than for the corresponding counterparts without gold, and as for total OSC, the increase observed in the case of gold-containing catalysts (382 and 496 $\mu mol_O/g$ for AuCuCe and AuCoCe, respectively) is much higher than for monometallic AuCe sample, which amounts to 131 $\mu mol_O/g$. As the real OSC accounts for the oxygen released only from ceria surface layers, these results suggest that the additional interface gold-copper or gold-cobalt present in gold-containing catalysts enhanced the spillover of CO to ceria surface.

The addition of either metal to the ceria surface substantially modified the reducibility of ceria during the OSC experiment, since the real OSCC values are considerably larger than for the bare ceria (the lowest increase of 34% for AuCe catalyst and the largest increase of 300% for AuCoCe catalyst), as well as the number of surface oxygen layers involved in the OSCC process. These results agree with the H_2-TPR experiments, where all the samples show reduction of the surface caps of ceria below 400 °C, as a consequence of the promoting effect of the metal oxides.

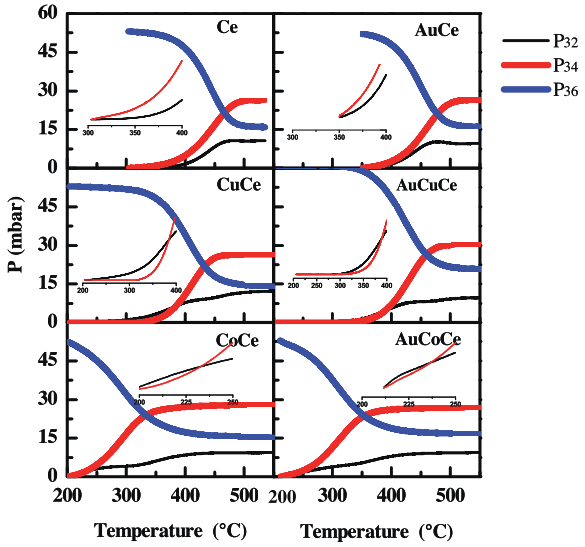

Fig. 4. Variation of the partial pressures of oxygen isotopomers during $^{18}O_2$ TPIE as a function of temperature.

3.2. Isotopic exchange

The evolutions as a function of the temperature of the $^{18}O_2$ (P_{36}), $^{18}O^{16}O$ (P_{34}) and $^{16}O_2$ (P_{32}) partial pressures monitored during the TPIE experiments on all the samples are represented in the Fig. 4. A magnification at the beginning of the exchange reaction was added (inset in the Fig. 4) in order to establish the type of oxygen exchange mechanism (simple or multiple) which governed the exchange process. Indeed this can be established from the analysis of the evolution of the partial pressures of the different isotopomers of oxygen (P_{32} and P_{34}), which is shown in Fig. 4. For Ce and AuCe samples, it is observed that both P_{34} and P_{32} start to increase at around 325–350 °C, P_{34} appearing in the gas phase slightly before P_{32}. It implies both simple and multiple mechanisms of exchange occur. This is a well known phenomenon for ceria since it was already reported that this oxide exchanges oxygen via the two types of mechanism [25]. Note that the presence of Au seems to delay the appearance of the $^{16}O_2$ and $^{18}O^{16}O$ molecules. On the contrary, the Fig. 4 clearly shows that the presence of Cu and Co allows a shift to the lower temperatures of the beginning of the exchange reaction. We also remark an inversion in the appearance of the products of the exchange, $^{16}O_2$ being the first molecule detected. It implies that there are oxygen anion vacancies in the materials which favor the multiple exchange by activating the O_2 molecules in the form of a diatomic species and leading to a decrease of the exchange threshold temperature [14]. Nevertheless, P_{34} increases much faster than P_{32} as the temperature increases, suggesting that the phenomenon previously described remains limited to the copper or cobalt clusters and their periphery. On the Co and Cu-containing catalysts, we also noted that the presence of gold seems to slightly delay the beginning of the exchange.

In order to compare the behavior of each sample in the TPIE experiment, we plotted in the Fig. 5 the variations with the temperature of the rate of exchange (Re) and of the number of oxygen species exchanged (Ne). The most representative results are also shown in Table 2.

It is worth noting that the Re_{max} will depend on the number of exchangeable atoms in the solids which is not the same for the different samples of the study. However, the initial concentration of oxygen in the solids will not strongly differ between AuCe and Ce, between AuCuCe and CuCe or between AuCoCe and CoCe in this study.

The maxima observed on the curves representing the rate of exchange versus the temperature is explained by the use of a closed system to perform the TPIE experiments. After the maxima, the rate

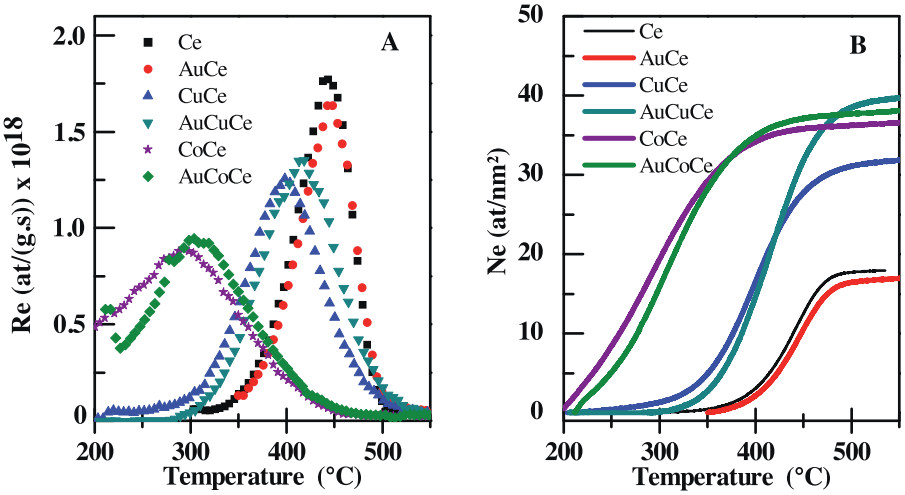

Fig. 5. (A) Evolution of the rate of oxygen exchange (Re) as a function of temperature; (B) Number of oxygen atoms exchanged (Ne) as a function of temperature.

Table 2
Results of TPIE experiments.

Catalyst	Exchangetemperature range (°C)	$T_{Surf,total}$ Exchange[a] (°C)	N_e[b] (at/nm^2)	T for$Re_{max\ (T_{max})}$ (°C)	Re_{max} (10^{+17}at/g_{cat} · s)	$N_{e,total}$[c] at/nm^2)
Ce	324–529	453	13.1	441	17.7	17.9
AuCe	350–556	469	14.1	448	16.3	17.2
CuCe	236–562	468	29.6	399	12.5	32.2
AuCuCe	289–553	473	36.1	419	13.4	39.7
CoCe	200*–508	369	39.4	295	11.0	46.1
AuCoCe	200*–507	412	43.2	302	12.1	46.9

[a] $T_{surf,total}$ exchange: Temperature for the complete exchange of the ceria surface.
[b] Number of oxygen atoms exchanged at $T_{surf,total}$; this value includes the oxygen atoms considering total exchange of Au_2O_3, Co_3O_4 and CuO.
[c] Total number of oxygen atoms exchanged at 550 °C.
* At the beginning of the experiment (200 °C) exchange already occurs.

of exchange which is proportional to the fraction of ^{18}O in the gas phase decreases. The rate becomes null when the equilibrium of ^{18}O concentration between the gas phase and the solid is reached. Bare ceria exchanges in a narrow range of temperatures (324–529 °C), similar to that reported in a previous study [2]. For the monometallic CoCe sample, which is more reducible than bare ceria, the exchange temperature range increases as it begins at lower temperature (less than 200 °C) while it finishes at 508 °C. Similarly, for the CuCe sample the exchange starts at lower temperature (236 °C) than bare ceria and finishes at 562 °C. Such a significant temperature decrease in cobalt- and copper-containing catalysts suggest both oxides promote the oxygen exchange in nanocrystalline ceria. Also, it is noticeable that for these samples the temperature interval where oxygen is exchanged widens in comparison with bare ceria. The curves corresponding to the gold-containing catalysts confirm that the presence of gold did not influence the temperature of exchange.

For the TPIE experiments the temperature of the maximum rate of exchange (T_{max}) decreases in the order AuCe ≈ Ce > AuCuCe ≈ CuCe > AuCoCe ≈ CoCe. The presence of copper and especially cobalt shift T_{max} to lower temperature in comparison with bare Ce and AuCe samples, which can be attributed to a spillover of oxygen from the oxide particles to the support [26]. For all the samples, in comparison with samples containing gold, their counterparts without gold show quite similar temperatures for the maximum rate of exchange, whereas they display slightly higher Re_{max}. AuCe sample shows lower Re_{max} than bare Ce, which matches the literature where the spillover effect in noble metal supported on reducible oxide systems is reported to be less intense that in non reducible supports [14]. The low adsorption coefficient of oxygen on gold particles [27] and the high barrier for the dissociation of adsorbed O_2 onto gold [28,29] can explain such an inhibitory effect of gold on ceria. The Re versus temperature plot for the AuCoCe sample (Fig. 5) shows two steps (low temperature peak, which is below 200 °C) and high temperature (at 302 °C), probably due to the existence of two mechanisms [30]. On the other hand the maximum rates of exchange (Re_{max}) for the gold-containing samples are larger than their corresponding counterparts without gold, which indicates that gold-containing catalysts are the most active for the exchange.

For all the samples the total number of oxygen atoms per surface area ($N_{e,total}$) exchanged up to 550 °C is shown in Table 2. All the values are slightly larger (about 2.6–6.7 at./nm^2) than the calculated amount of surface oxygen. In fact, for all the samples the surface oxygen atoms are already totally exchanged by the temperatures $T_{Surf,total}$ given Table 2, which implies that during TPIE experiments, surface oxygen species and part of the bulk oxygen species are both exchanged without any change observed in the mechanism (as seen below, where no exchange in the variation of the isotopomers partial pressures is observed). Regarding $N_{e,total}$, the catalysts can be allocated in three groups: the cobalt-containing samples, with the highest $N_{e,total}$, the intermediate $N_{e,total}$ for copper-containing samples, and the lowest $N_{e,total}$ for the Ce and AuCe samples.

3.3. $C^{16}O$ oxidation and exchange

$C^{16}O$ oxidation and exchange were investigated over ^{18}O pre-exchanged catalysts. The $^{18}O/^{16}O$ pre-exchange was performed in order to have a number of ^{18}O atoms equal to one layer of ceria crystallites plus the O atoms of the metal-oxide particles (assuming that oxygen atoms from Au_2O_3, CuO and Co_3O_4 exchange completely and in preference). Then we studied the reactivity of surface oxygen atoms and the oxygen availability from the samples by carrying out two isothermal experiments, both feeding $C^{16}O$: one anaerobic oxidation, where $C^{16}O$ was diluted with Ar; and the other aerobic oxidation, where $C^{16}O$ was mixed with O_2.

When $C^{16}O$ is introduced, the oxygen exchange reaction would be:

$$C^{16}O_g + {}^{18}O_s \rightarrow C^{18}O_g + {}^{16}O_s \quad (5)$$

For CO oxidation, assuming that all the reacting CO gives CO_2(g) and that all formed CO_2 comes from CO(g), the only possible reactions are:

$$C^{16}O_g + 1/2\,{}^{16}O_{2g} \rightarrow C^{16}O_{2g} \quad (6)$$

$$C^{16}O_g + {}^{16}O_s \rightarrow C^{16}O_{2g} \quad (7)$$

$$C^{16}O_g + {}^{18}O_s \rightarrow C^{16}O^{18}O_g \quad (8)$$

$$C^{18}O_g + {}^{16}O_s \rightarrow C^{18}O^{16}O_g \quad (9)$$

$$C^{18}O_g + {}^{18}O_s \rightarrow C^{18}O_{2g} \quad (10)$$

At high temperature both the exchange reaction (Reaction (5)) and $C^{16}O$ oxidation reaction (Reactions (6–10)) occur at high rates. Accordingly, the evolution of different gas-phase compounds is very fast making difficult the discrimination among different mechanisms. For this reason, an intermediate temperature of 130 °C was chosen, which is representative temperature for CO-PROX reaction. The time evolution of the partial pressure of the reactant ($C^{16}O$) as a function of time are shown in Figs. 6 and 7 , for $C^{16}O$/Ar and $C^{16}O/^{16}O_2$ feeds, respectively.

No release of hydrogen was detected during the experiments, which suggests that CO did not react with residual surface hydroxyl groups via WGS. It is worth noting that in the $C^{16}O/^{16}O_2$ experiments, partial pressures of $^{16}O^{18}O$ and $^{18}O_2$ were not detected. For each experiment, the quantification of CO transformation, CO_2 production, ratio between the initial rate of exchange and the initial rate of oxidation as well as between the initial amount of $C^{16}O_2$ and $C^{16}O^{18}O$ was made. All the values are reported in Table 3.

In anaerobic conditions, as no gas phase oxygen is being fed, the oxygen which would participate in reactions 5–10 comes from the catalyst surface (Reaction (6) cannot occur). In these conditions, bare ceria has nil activity in CO oxidation. The active participation of lattice oxygen for gold catalysts supported on reducible oxides

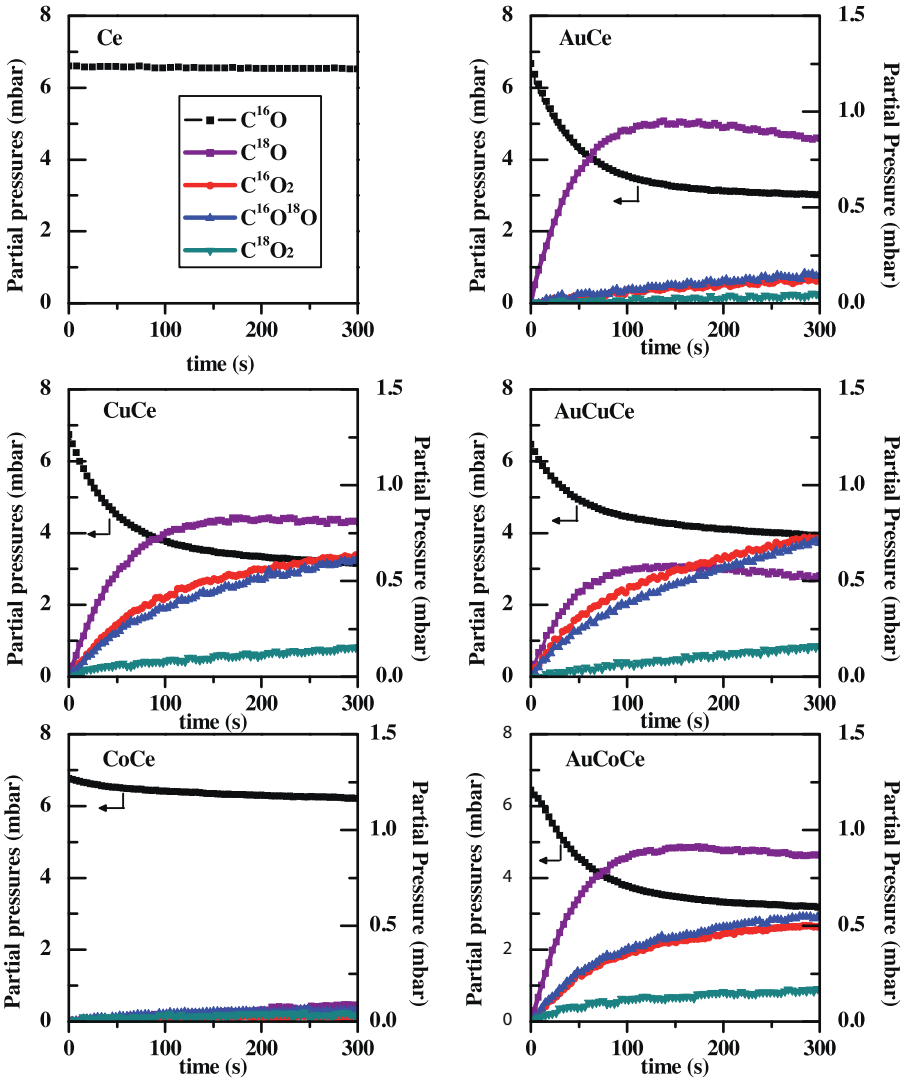

Fig. 6. Evolution of the partial pressures of CO and CO_2 isotopomers as a function of time during anaerobic $C^{16}O$ oxidation ($C^{16}O$/Ar).

is already reported in literature [31] as well as for copper or cobalt catalysts [32,33]. Therefore, in the absence of dioxygen in the gas phase, the production of CO_2 observed in the Fig. 6 may be linked to the OSC and OSCC values obtained previously. For gold supported onto reducible oxides close correlation between OSC and reactivity has been reported [34], which means that reaction occurs at the perimeter of gold nanoparticles [35]. The catalytic activity of noble metal catalysts is often correlated with metal/oxide interfacial perimeter [36], which can be extended for transition metal–ceria samples [37], as deduced from the activity of both CuO/ceria and inverse ceria/CuO catalysts. Similarly, the gold/oxide interfacial perimeter is often the location of the activation of oxygen [38,39] of supported gold catalysts. The heterogeneity of our samples, where Au is supported on different surfaces (ceria, CuO and cobalt, and combination of them), and the contribution to the catalytic activity of the transition metal oxide-ceria perimeter [27,40] makes unfeasible to discuss the activity in terms of perimeter length. It can be seen that the rate of CO_2 production for AuCe and CoCe catalysts is very low. Contrary to CoCe, the results could be expected for AuCe after considering the OSC value measured at 400 °C. At lower temperature the absence of CO_2 production could then be anticipated. Nevertheless the experiment brings new information since it shows that for this sample the $C^{16}O/C^{18}O$ exchange is very rapid. At 130 °C, release of oxygen from AuCe catalyst is

Table 3
Surface activity (as $C^{16}O$ fractional conversion); CO_2 ($\mu mol_{CO2}/g_{cat}$) formed by direct oxidation (given as $C^{16}O_2 + C^{16}O^{18}O + C^{18}O_2$) at 300 s of reaction; rate of exchange/rate of oxidation at $t = 0$; $C^{16}O_2/C^{16}O^{18}O$ at $t = 0$; fractional CO conversion and selectivity towards CO_2 in CO-PROX reaction at 130 °C.

Catalysts	Surface activity		CO_2 formation		$[r_{exchange}/r_{oxidation}]_{t=0}$		$[C^{16}O_2/C^{16}O^{18}O]_{t=0}$		CO-PROX	
	$C^{16}O$/Ar	$C^{16}O/O_2$	$C^{16}O$/Ar	$C^{16}O/O_2$	$C^{16}O$/Ar	$C^{16}O/O_2$	$C^{16}O$/Ar	$C^{16}O/O_2$	X_{CO}	S_{CO2}
Ce	~0	~0	~0	~0	–	–	–	–	0.04	~1
AuCe	0.57	0.59	27.0	291.6	16.8	1.0	0.9	0.4	0.31	1
CuCe	0.51	0.87	133.9	451.2	1.2	1.0	1.2	1.4	0.42	1
AuCuCe	0.44	0.80	151.3	466.8	0.8	~0	1.4	1.4	0.46	1
CoCe	0.09	0.66	10.2	368.5	0.8	0.04	0.5	0.9	0.36	1
AuCoCe	0.50	0.83	107.9	498.0	1.5	0.03	1.0	2.7	0.45	1

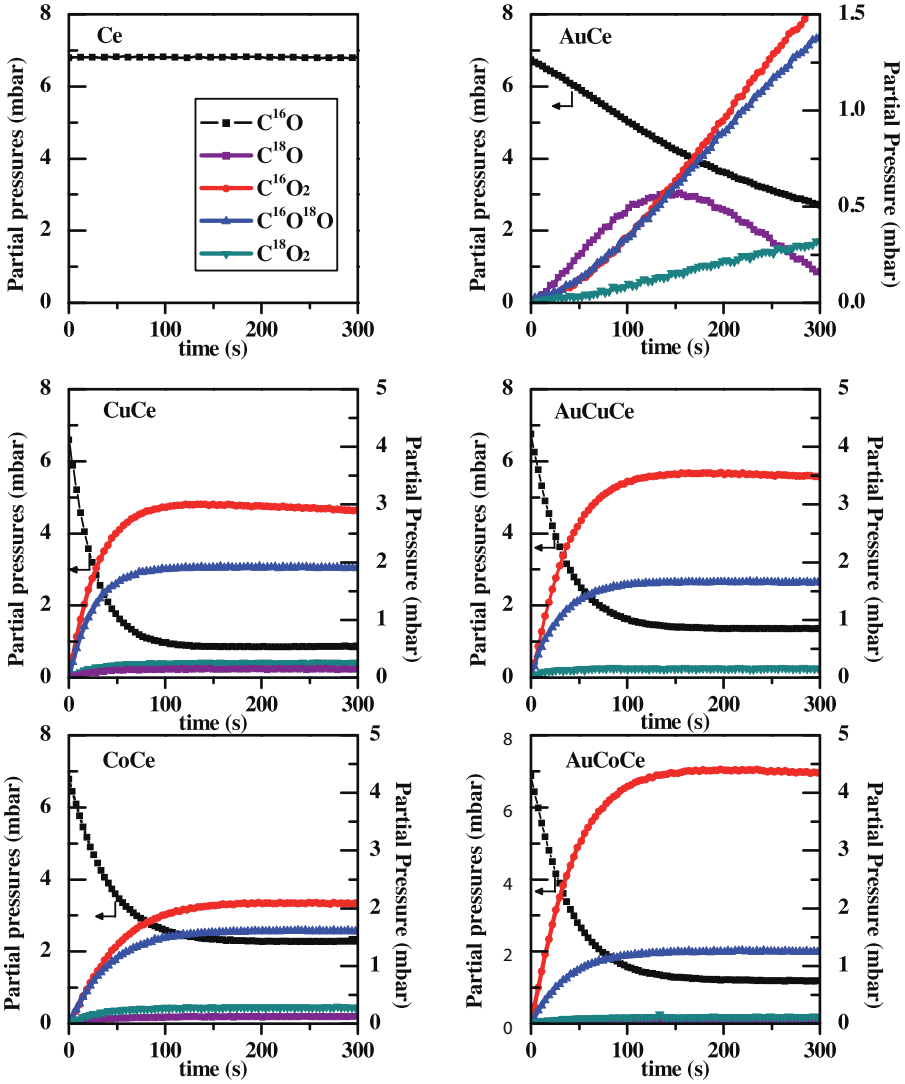

Fig. 7. Evolution of the partial pressures of CO and CO_2 isotopomers as a function of time during aerobic $C^{16}O$ oxidation ($C^{16}O/O_2$).

not possible although some of the oxygen surface atoms participate to the exchange with gas phase CO. For CoCe sample the high OSC measured at 400 °C does not appear at 130 °C, the production of CO_2 being almost null. The evolution of the partial pressures curves also shows that the exchange does not occur with this sample as it could be observed for bare CeO_2 (not shown here). Gold, contrary to cobalt particles, plays a role in the exchange of oxygen species between CO and framework oxygen atoms. It is not only due to the capacity of Au to adsorb CO molecules since CO can be adsorbed also on cobalt oxide particles [41]. When Au is added to CoCe catalyst, the activities in both oxidation and exchange reactions increase dramatically and the value characterizing the $C^{16}O$ conversion is enhanced by a factor of 5.5 whereas the amount of CO_2 produced is enhanced by a factor of 4 from AuCe to AuCoCe. The higher activity in oxidation is then the result of a synergistic effect between cobalt and gold as has been observed in OSC measurements. In this catalytic system co-exist both gold on ceria and gold on cobalt entities, in both cases with different particle size distribution, which might enhance the synergism between Au–Co–Ce. The case of CuCe catalyst is again different: this sample is able to produce CO_2 (133.9 $\mu mol_{CO2}/g$) and to exchange the oxygen atom of CO. It matches well with the OSC which showed that the oxygen storage/release capacity was in major part due to the copper oxidation/reduction. One can conclude that at 130 °C CO is able to reduce CuO to give CO_2. The addition of gold to the CuCe sample slightly modifies the behavior of the solid promoting the oxidation reaction to the detriment of the exchange. This could be due to the lower surface area of AuCuCe sample with respect to CuCe. It can be concluded that the exchange reaction is proportional to the ceria surface whereas the CO oxidation reaction is directly linked to the copper content. In our samples, the presence of gold promotes the reduction of ceria, copper and cobalt species, as clearly seen by TPR (Fig. 3), which occurs by weakening of the metal-oxide bond [42].

In aerobic conditions, $C^{16}O$ can react with both gas phase dioxygen and lattice oxygen atoms. Moreover the exchange phenomenon previously observed in anaerobic conditions can also proceed. Fig. 7 shows the evolution of the partial pressures of the reactant ($C^{16}O$) and of the different products as a function of time. It is worth noting that the experiments were performed in a large excess of $^{16}O_2$ (the molar ratio CO/O_2 was around 0.14). As in anaerobic condition, bare ceria has nil activity in CO oxidation. We increased the temperature to check the beginning of CO oxidation on bare ceria, which is found to occur around 250 °C. As far as the dioxygen isotopomers are concerned (not showed in the Figures) one can say that $^{16}O_2$ partial pressure very slightly decreases as a function of time while $^{16}O^{18}O$ and $^{18}O_2$ partial pressures remain null during all the experiments. It shows that the direct oxygen exchange does not take place at 130 °C. As expected, the activities observed in aerobic

oxidation are considerably higher than in anaerobic experiments. Among the samples the AuCe catalyst exhibits the lowest activity. The ratio between the initial rate of exchange and the initial rate of oxidation ($[r_{exchange}/r_{oxidation}]_{t=0}$), given in Table 3, is equal to 1 but the evolution of the curves for this sample show that the exchange is predominant. The fact that a maximum appears in the curve corresponding to the $C^{18}O$ partial pressure indicates that the CO molecule is exchanged before being oxidized. The behavior of the other catalysts is quite different with a rapid oxidation reaction and the absence of $C^{18}O$ in the gas phase contrary to what was observed in anaerobic conditions for CuCe, AuCuCe and AuCoCe. Nevertheless, despite the large excess of $^{16}O_2$, it can be seen that fraction of the ^{18}O atoms present in the pre-exchanged samples appears in the CO_2 produced. The ratio between the initial amount of $C^{16}O_2$ and $C^{16}O^{18}O$ produced is close to 1 except for AuCoCe which exhibits a ratio of 2.7. It demonstrates that even at low temperatures the lattice oxygen can participate in the CO oxidation mechanism. One can conclude that the CO when exchanged in CuCe, AuCuCe and AuCoCe is oxidized before being desorbed into the gas phase. The case of CoCe catalyst is specific inasmuch as in the presence of large excess of normal oxygen $C^{16}O^{18}O$ is produced even though the exchange was not observed in anaerobic conditions. Indeed, compared to anaerobic conditions, the activity of CoCe increased substantially. It is documented that in the presence of gas phase oxygen, Co_3O_4 catalyst is extraordinary oxidation catalysts, in both supported and bulk configurations, even at sub-ambient temperature [41]. One explanation could come from the fact that the formation of carbonate species favored in presence of oxygen could be the intermediates in the exchange [23]. Finally we observe that CuCe, AuCuCe and AuCoCe are the most active catalysts and no further conversion of CO occurs beyond 150 s. A difference in the ratio $C^{16}O_2$ /$C^{16}O^{18}O$ produced is apparent. After 300 s we observe the following ranking CuCe < AuCuCe < AuCoCe. Surprisingly the ranking is inversely proportional to the number of ^{18}O available in the catalytic surface. It means that AuCoCe, which possesses the higher loading of ^{18}O atoms initially, gives the higher amount of $C^{16}O_2$ after CO oxidation reaction. This result is explained by the capacity of AuCoCe to exchange ^{16}O at the lowest temperature, as seen in the TPIE experiments.

3.4. CO-PROX activity at 130 °C

The performance of the catalysts in CO-PROX reaction was measured at $\lambda = 0.48$ (less oxygen than the required for complete CO conversion) at 130 °C, and the obtained fractional CO conversions and selectivities toward CO_2 are given in Table 3. With this λ value, and in the absence of any parallel reactions such as H_2 oxidation or WGS, the maximum CO conversion achievable without the releasing of the lattice oxygen is 0.48. This means that some of the catalysts (AuCe, AuCuCe and AuCoCe) are close to this maximum. It is worth to note that bare ceria converted around 4% of CO, with almost complete selectivity toward CO_2. Indeed, at this temperature all the catalysts showed complete selectivity toward CO_2. Clearly, the addition of transition metal or gold enhanced the activity in CO-PROX. Moreover, the presence of both gold and transition metal oxide enhanced the catalysts activity with respect the gold-free catalysts, in good agreement with the results in aerobic CO oxidation over ^{18}O pre-exchanged catalysts, confirming the synergistic effect of gold and transition metal oxide for CO oxidation at 130 °C.

On Au/ceria supports, surface oxygen species which are active for both CO and H_2 oxidation are identical, both gases competing for the active site during reaction [43]. Moreover, hydrogen promotes the oxidation of CO in CO-PROX reaction conditions [44]. This can explain the 100% selectivity toward CO_2 obtained by this catalyst. In very remarkable work Gamarra et al. [45] reported two

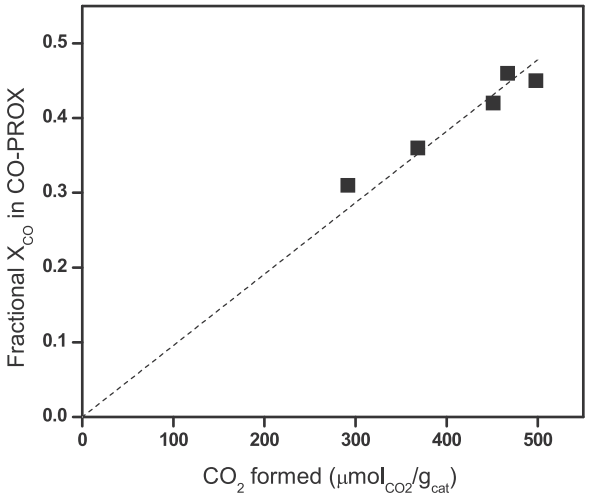

Fig. 8. Fractional CO conversion in CO-PROX in function of CO_2 ($\mu mol_{CO2}/g_{cat}$) formed by direct oxidation (given as $C^{16}O_2 + C^{16}O^{18}O + C^{18}O_2$) at 300 s of reaction during anaerobic (open symbols) and aerobic (full symbols) $C^{16}O$ oxidation.

distinct active sites for CO and H_2 oxidation on copper–ceria catalysts: the interfacial Cu–Ce sites for CO, and copper particles upon extension of their reduction from the interface for H_2·H_2-TPR of copper-containing samples showed that at 130 °C the reduction of copper is limited to Cu^{1+} in the surroundings of interface, which leads the complete selectivity to CO_2 in CO-PROX of these samples. In cobalt-based catalysts, Co^{3+} species are the most active for CO oxidation. Moreover, large cobalt entities oxidize selectively CO in the presence of hydrogen [46]. Therefore, the complete selectivity of cobalt catalysts can be explained by the size of cobalt particles, as found by HRTEM.

Fig. 8 shows the activity in CO-PROX in function of activity in both aerobic and anaerobic $C^{16}O$ oxidation after exchange. As expected, a linear correlation was found when plotted against aerobic oxidation, as the selectivity toward CO_2 is complete in CO-PROX reaction for all the supported catalysts. However, X_{CO} in CO-PROX does not correlate with the anaerobic CO oxidation, which can be explained by the different mechanisms to release the lattice oxygen of our samples.

4. Conclusions

In this work the rate of exchange of $^{18}O/^{16}O$ species over monometallic CuO/CeO_2 and Co_3O_4/CeO_2 catalysts, and Au–CuO/CeO_2 and Au–Co_3O_4/CeO_2 catalysts was measured. Also, both the anaerobic and aerobic oxidation of carbon monoxide over ^{18}O-preoxidized catalysts has been studied at 130 °C. For all the samples, both real and total OSC and OSCC increased with the incorporation of gold, which suggests a synergistic effect in the interface between gold species and metal oxides (CuO or Co_3O_4), stronger than in the gold–ceria interface.

TPIE experiments carried out at catalysts with and without gold allow determination of both the temperature range and the mechanism of oxygen isotopic exchange. The samples exchange oxygen in the following order of temperature (temperature of the maximal rate of exchange): CoCe ≈ AuCoCe < CuCe ≈ AuCuCe < Ce ≈ AuCe.

The CO oxidation experiments performed in ^{18}O atom-containing catalysts allow us to demonstrate that the reaction involves lattice oxygen atoms even at temperatures where exchange of gaseous oxygen alone is not possible. Depending on the nature of the catalyst, the framework oxygen atoms participate either in oxidizing the CO adsorbed molecule or in being exchanged with CO reactant or CO_2 product. In anaerobic CO oxidation, the

exchange is fast and is almost the only reaction observed to occur over AuCe catalyst, while little activity is detected over CoCe sample. Monometallic CuCe sample is by far the most active catalyst in oxidation and is also active in exchange reaction. The results obtained for the AuCoCe catalyst are the consequence of a synergistic effect between Au, Ce and Co which is not observed for the AuCuCe catalyst. In aerobic CO oxidation, for all the samples containing copper or cobalt, the oxidation is the fastest reaction in the whole time of the experiment. The activity in CO oxidation follows the ranking AuCe < < CoCe < CuCe ≈ AuCuCe < AuCoCe, confirming the synergistic effect of gold and cobalt. The activity in CO-PROX of supported monometallic and bimetallic catalysts shows linear correlation with the activity in aerobic $C^{16}O$ oxidation after exchange.

Acknowledgements

Authors wish to thank Spanish MEC (Project ENE2007-67975) for the financial support. N.G. thanks the MEC for her grant. Also, the authors thank for technical and human support provided by SGIker of UPV/EHU. Junta de Andalucía (Grant Number P10-FQM-6766, Groups FQM-110 and FQM-334).

References

[1] D. Duprez, Appl. Catal. A: Gen. 82 (1992) 111–157.
[2] Y. Madier, C. Descorme, A.M. Le Govic, D. Duprez, J. Phys. Chem. B 103 (1999) 10999–11006.
[3] H.C. Yao, Y.F. Yu Yao, J. Catal. 86 (1984) 254–265.
[4] L.T. Weng, B. Delmon, Appl. Catal. A: Gen. 81 (1992) 141–213.
[5] S. Ojala, N. Bion, S. Rijo Gomes, R.L. Keiski, D. Duprez, ChemCatChem 2 (2010) 527–533.
[6] C. Descorme, D. Duprez, Appl. Catal. A: Gen. 202 (2000) 231–241.
[7] S.Y. Christou, A.M. Efstathiou, Top. Catal. 56 (2013) 232–238.
[8] K.C. Petallidou, A.M. Efstathiou, Appl. Catal. B: Environ. 140–141 (2013) 333–347.
[9] T. Ramírez-Reina, A. Álvarez-Moreno, S. Ivanova, J.A. Odriozola, M.A. Centeno, ChemCatChem 4 (2012) 512–520.
[10] D.I. Potemkin, E.Y. Semitut, Y.V. Shubin, P.E. Plyusnin, P.V. Snytnikov, E.V. Makotchenko, D.Y. Osadchii, D.A. Svintsitskiy, S.A. Venyaminov, S.V. Korenev, V.A. Sobyanin, Catal. Today 235 (2014) 103–111.
[11] N.K. Gamboa-Rosales, J.L. Ayastuy, M.P. González-Marcos, M.A. Gutiérrez-Ortiz, Int. J. Hydrogen Energy 37 (2012) 7005–7016.
[12] S. Bernal, F.J. Botana, J.J. Calvino, C. Lopez-Cartes, J.A. Perez-Omil, J.M. Rodriguez-Izquierdo, Ultramicroscopy 72 (1998) 135–164.
[13] D. Duprez, C. Descorme, Catalysis by Ceria and Related Materials, in: A. Trovarelli (Ed.), Imperial College Press, London, 2002, pp. 243–280.
[14] D. Martin, D. Duprez, J. Phys. Chem. 100 (1996) 9429–9438.
[15] G.K. Boreskov, The Catalysis of Isotopic Exchange in Molecular Oxygen. Advances in Catalysis, in: D.D. Eley (Ed.), Academic Press, Amsterdam, 1965, pp. 285–339.
[16] C. Kleinlogel, L.J. Gauckler, Solid State Ionics 135 (2000) 567–573.
[17] L. Delannoy, K. Fajerwerg, P. Lakshmanan, C. Potvin, C. Méthivier, C. Louis, Appl. Catal. B: Environ. 94 (2010) 117–124.
[18] Q. Fu, W. Deng, H. Saltsburg, M. Flytzani-Stephanopoulos, Appl. Catal. B: Environ. 56 (2005) 57–68.
[19] F. Arena, P. Famulari, G. Trunfio, G. Bonura, F. Frusteri, L. Spadaro, Appl. Catal. B: Environ. 66 (2006) 81–91.
[20] A. Pintar, J. Batista, S. Hocevar, S. J. Colloid Interface Sci. 285 (2005) 218–231.
[21] G. Avgouropoulos, T. Ioannides, H. Matralis, Appl. Catal. B: Environ. 56 (2005) 87–93.
[22] J.Y. Luo, M. Meng, X. Li, X.G. Li, Y.Q. Zha, T.D. Hu, Y.N. Xie, J. Zhang, J. Catal. 254 (2008) 310–324.
[23] Y.W. Chen, H.J. Chen, D.S. Lee, J. Mol. Catal. A: Chem. 363–364 (2012) 470–480.
[24] H.C. Yang, F.W. Chang, L.S. Roselin, J. Mol. Catal. A: Chem. 276 (2007) 184–190.
[25] D. Duprez, Isotopes in heterogeneous Catalysis, in: J.S.J. Hargreaves, S. David Jackson, G. Webb (Eds.), Catalytic Science Series 4, Imperial College Press, London, 2006, pp. 133–181.
[26] P.A. Kumar, M.D. Tanwar, N. Russo, R. Pirone, D. Fino, Catal. Today 184 (2012) 279–287.
[27] J. Fonseca, H.S. Ferreira, N. Bion, L. Pirault-Roy, M.D.C. Rangel, D. Duprez, F. Epron, Catal. Today 180 (2012) 34–41.
[28] D. Widmann, R.J. Behm, Angew. Chem. Int. Ed. 50 (2011) 10241–10245.
[29] Z.P. Liu, P. Hu, A. Alavi, J. Am. Chem. Soc. 124 (2002) 14770–14779.
[30] W. Yang, R. Zhang, B. Chen, N. Bion, D. Duprez, S. Royer, J. Catal. 295 (2012) 45–58.
[31] D. Widmann, R. Leppelt, R.J. Behm, J. Catal. 251 (2007) 437–442.
[32] A. Gurbani, J.L. Ayastuy, M.P. González-Marcos, M.A. Gutiérrez-Ortiz, Int. J. Hydrogen Energy 35 (2010) 11582–11590.
[33] X. Xu, J. Li, Z. Hao, J. Rare Earth 24 (2006) 172–176.
[34] D. Widmann, Y. Liu, F. Schüth, R.J. Behm, J. Catal. 276 (2010) 292–305.
[35] I.X. Green, W. Tang, M. Neurock, J.T. Yates, Science 333 (2011) 736–739.
[36] C.M. Kalamaras, D.D. Dionysiou, A.M. Efstathiou, ACS Catal. 2 (2012) 2729–2742.
[37] J.C. Hanson, R. Si, W. Xu, S.D. Senanayake, K. Mudiyanselage, D. Stacchiola, J.A. Rodriguez, H. Zhao, K.A. Beyer, G. Jennings, K.W. Chapman, P.J. Chupas, A. Martínez-Arias, Catal. Today 229 (2014) 64–71.
[38] Y.Y. Wu, N.A. Mashayekhi, H.H. Kung, Catal. Sci. Technol. 3 (2013) 2881–2891.
[39] M. Kotobuki, R. Leppelt, D.A. Hansgen, D. Widmann, R.J. Behm, J. Catal. 264 (2009) 67–76.
[40] N. Qiu, J. Zhang, Z. Wu, Phys. Chem. Chem. Phys. 16 (2014) 22659–22664.
[41] Y. Lou, X.M. Cao, J. Lan, L. Wang, Q. Dai, Y. Guo, J. Ma, Z. Zhao, Y. Guo, P. Hu, G. Lu, Chem. Commun. 50 (2014) 6835–6838.
[42] Y. Chen, P. Hu, M.H. Lee, H. Wang, Surf. Sci. 602 (2008) 1736–1741.
[43] L.C. Wang, D. Widmann, R.J. Behm, Catal. Sci. Technol., 2015, Adv. Article (2015), http://dx.doi.org/10.1039/c4cy0130b.
[44] E. Quinet, L. Piccolo, F. Morfin, P. Avenier, F. Diehl, V. Caps, J.L. Rousset, J. Catal. 268 (2009) 384–389.
[45] D. Gamarra, C. Belver, M. Fernández-García, A. Martínez-Arias, J. Am. Chem. Soc. 129 (2007) 12064–12065.
[46] P. Gawade, B. Bayram, A.M.C. Alexander, U.S. Ozkan, Appl. Catal. B: Environ. 128 (2012) 21–30.